







Cite this: *Phys. Chem. Chem. Phys.*,  
2021, 23, 22437

# Shock wave and modelling study of the unimolecular dissociation of $\text{Si}(\text{CH}_3)_2\text{F}_2$ : an access to spectroscopic and kinetic properties of $\text{SiF}_2^\dagger$

C. J. Cobos, <sup>a</sup> L. Sölter, <sup>bc</sup> E. Tellbach <sup>bc</sup> and J. Troe <sup>\*bc</sup>

The thermal dissociation of  $\text{Si}(\text{CH}_3)_2\text{F}_2$  was studied in shock waves between 1400 and 1900 K. UV absorption-time profiles of its dissociation products  $\text{SiF}_2$  and  $\text{CH}_3$  were monitored. The reaction proceeds as a unimolecular process not far from the high-pressure limit. Comparing modelled and experimental results, an asymmetric representation of the falloff curves was shown to be most realistic. Modelled limiting high-pressure rate constants agreed well with the experimental data. The UV absorption spectrum of  $\text{SiF}_2$  was shown to be quasi-continuous, with a maximum near 222 nm and a wavelength-integrated absorption cross section of  $4.3 (\pm 1) \times 10^{-23} \text{ cm}^3$  (between 195 and 255 nm, base e), the latter being consistent with radiative lifetimes from the literature. Experiments over the range 1900–3200 K showed that  $\text{SiF}_2$  was not consumed by a simple bond fission  $\text{SiF}_2 \rightarrow \text{SiF} + \text{F}$ , but by a bimolecular reaction  $\text{SiF}_2 + \text{SiF}_2 \rightarrow \text{SiF} + \text{SiF}_3$  (rate constant in the range  $10^{11}$ – $10^{12} \text{ cm}^3 \text{ mol}^{-1} \text{ s}^{-1}$ ), followed by the unimolecular dissociation  $\text{SiF}_3 \rightarrow \text{SiF}_2 + \text{F}$  such that the reaction becomes catalyzed by the reactant  $\text{SiF}_2$ . The analogy to a pathway  $\text{CF}_2 + \text{CF}_2 \rightarrow \text{CF} + \text{CF}_3$ , followed by  $\text{CF}_3 \rightarrow \text{CF}_2 + \text{F}$ , in high-temperature fluorocarbon chemistry is stressed. Besides the high-temperature absorption cross sections of  $\text{SiF}_2$ , analogous data for  $\text{SiF}$  are also reported.

Received 19th July 2021,  
Accepted 22nd September 2021

DOI: 10.1039/d1cp03298d

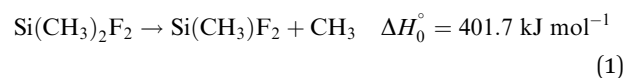
rsc.li/pccp

## Introduction

The role of  $\text{SiF}_2$  in the etching of silicon by fluorine atoms continues to be under debate (see, for example, the review in ref. 1). Part of the problem lies in the scarcity of quantitative information on the properties of this intermediate in chemical or plasma-assisted etching processes employing fluorine-containing compounds. A limited amount of kinetic data is available for room temperature conditions (e.g., ref. 2–6), while less is known for elevated temperatures. The present article intends to improve this situation by investigating kinetic properties of  $\text{SiF}_2$  under high-temperature conditions in shock waves.

First, a suitable source for  $\text{SiF}_2$  had to be selected. It has been shown that the thermal dissociation of  $\text{Si}_2\text{F}_6$ , in a process  $\text{Si}_2\text{F}_6 \rightarrow \text{SiF}_2 + \text{SiF}_4$  and with a rate constant  $10^{12.41} \exp(-193.5 \text{ kJ mol}^{-1}/RT) \text{ s}^{-1}$ , directly produces  $\text{SiF}_2$ .<sup>7,8</sup> The thermal dissociation of  $\text{SiF}_4$ , on the other hand, in a

sequence  $\text{SiF}_4 \rightarrow \text{SiF}_3 \rightarrow \text{SiF}_2$  also leads to  $\text{SiF}_2$ , but, because of the large thermal stability of  $\text{SiF}_4$ , requires considerably higher temperatures than the dissociation of  $\text{Si}_2\text{F}_6$ . In the present work, instead of  $\text{Si}_2\text{F}_6$  or  $\text{SiF}_4$ , it appeared more suitable to use  $\text{Si}(\text{CH}_3)_2\text{F}_2$  as the precursor for  $\text{SiF}_2$ . This compound is easy to handle in shock wave experiments and, at comparably low temperatures, it forms  $\text{SiF}_2$  in a sequence of the two steps



(the given reaction enthalpies at 0 K,  $\Delta H_0^\circ$ , were determined by quantum-chemical calculations as described in the ESI†).

Next, a detection method for  $\text{SiF}_2$  had to be chosen. As the UV absorption of  $\text{CF}_2$  has been found useful to study high-temperature fluorocarbon chemistry,<sup>9–11</sup> one may try to employ the analogous spectrum of  $\text{SiF}_2$  to investigate reactions of the latter. At room temperature,  $\text{SiF}_2$  has a band spectrum which is similarly structured and intense as that of  $\text{CF}_2$ .<sup>13</sup> One may expect that this spectrum at high temperatures becomes similarly quasi-continuous as that of  $\text{CF}_2$ . One of the goals of the present work, therefore, was the characterization of the UV absorption spectrum of  $\text{SiF}_2$  at elevated temperatures and to

<sup>a</sup> INIFTA, Facultad de Ciencias Exactas, Universidad Nacional de La Plata, CONICET, Argentina

<sup>b</sup> Institut für Physikalische Chemie, Universität Göttingen, Tammannstrasse 6, D-37077 Göttingen, Germany

<sup>c</sup> Max-Planck-Institut für Biophysikalische Chemie, Am Fassberg 11, D-37077 Göttingen, Germany. E-mail: juergen.troe@mpibpc.mpg.de

† Electronic supplementary information (ESI) available. See DOI: 10.1039/d1cp03298d



determine its absorption cross section as a function of temperature and wavelength in comparison to quantum-chemical calculations of its oscillator strength (as described in the ESI†).

There are more aspects of the present work. Monitoring  $\text{SiF}_2$  formation in reactions (1) and (2) enables one to follow the unimolecular dissociation reaction of  $\text{Si}(\text{CH}_3)_2\text{F}_2$ . This molecule is sufficiently large to dissociate (under typical shock wave conditions) not far from the high-pressure limit of the unimolecular reaction. Therefore, a study of the pressure dependence of the dissociation rate constant  $k$  appears suitable to analyze its approach to the high-pressure rate constant  $k_\infty$ . This is an issue in standard unimolecular rate theory. The various versions of the latter propose different approaches of  $k$  to  $k_\infty$ .<sup>14,15</sup> By comparing experimental and modelled rate constants, the present study provides an opportunity to address this problem in particular detail. In addition, in high-temperature fluorocarbon chemistry an autocatalytic pathway for  $\text{CF}_2$  decomposition of the type  $\text{CF}_2 + \text{CF}_2 \rightarrow \text{CF} + \text{CF}_3$ , followed by  $\text{CF}_3 \rightarrow \text{CF}_2 + \text{F}$ , was observed.<sup>11</sup> It appears of interest to search for an analogous pathway  $\text{SiF}_2 + \text{SiF}_2 \rightarrow \text{SiF} + \text{SiF}_3$ , followed by  $\text{SiF}_3 \rightarrow \text{SiF}_2 + \text{F}$ , in high-temperature fluorosilicon chemistry. In both cases, the very endothermic direct dissociation of  $\text{CF}_2$  or  $\text{SiF}_2$ , respectively, then can be circumvented by a faster mechanism which also leads to dissociation.

### Experimental technique and results

The present experiments have been performed by heating mixtures of  $\text{Si}(\text{CH}_3)_2\text{F}_2$  and Ar in shock waves.  $\text{Si}(\text{CH}_3)_2\text{F}_2$  (from abcr with a purity of 99%) could be used without further purification, because it was highly diluted (down to about 30 ppm) in the bath gas Ar (from Air Liquide with a purity of 99.9999%). The shock tube, as well as the UV lamp – quartz monochromator – photomultiplier – data acquisition equipment for recording absorption-time profiles, have, *e.g.*, been detailed in ref. 11 and 16 such that no further description is given here. In the first part of the present experiments, absorption-time profiles of shock-heated mixtures of about 100 ppm of  $\text{Si}(\text{CH}_3)_2\text{F}_2$  in Ar were recorded at the wavelength of 222 nm, *i.e.* near to the maximum of the room-temperature absorption of  $\text{SiF}_2$ .<sup>12</sup> Fig. 1 shows an example for a temperature of 1660 K behind the reflected shock wave. Directly behind the Schlieren peaks of the incident and reflected shock waves, no absorption signal is observed. This indicates that the absorption continuum of the parent molecule  $\text{Si}(\text{CH}_3)_2\text{F}_2$  (having a room-temperature maximum near 155 nm<sup>17</sup>) with increasing temperature does not broaden to such an extent that it would influence absorption measurements at 222 nm. The absorption signal of Fig. 1 then can directly be related to the formation of  $\text{SiF}_2$  (as reaction (1) is by far more endothermic than reaction (2),  $\text{Si}(\text{CH}_3)_2\text{F}_2$  should rapidly dissociate to  $\text{CH}_3 + \text{SiF}_2$ ). One may also look for an absorption signal from  $\text{CH}_3$ . It is known that there is an absorption band of  $\text{CH}_3$  not far from that of  $\text{SiF}_2$ . However, its maximum is located at shorter wavelengths (near to 215 nm) and its maximum absorption cross section is much smaller than that of  $\text{SiF}_2$ .<sup>18</sup> Because the absorption

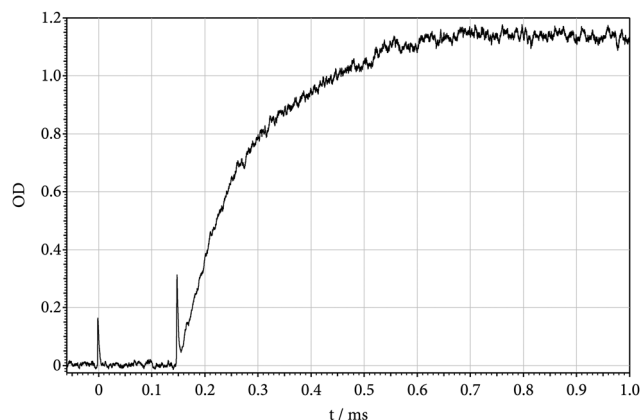


Fig. 1 Absorption-time profile at 222 nm of  $\text{SiF}_2$  forming by unimolecular dissociation of  $\text{Si}(\text{CH}_3)_2\text{F}_2$  behind reflected shock wave ( $T = 1660$  K,  $[\text{Ar}] = 8.6 \times 10^{-5} \text{ mol cm}^{-3}$ , 100 ppm of  $\text{Si}(\text{CH}_3)_2\text{F}_2$  in Ar;  $\text{OD} = \sigma[\text{SiF}_2]$  with  $l = 9.4$  cm).

cross section of  $\text{SiF}_2$  decreases with decreasing wavelength, a signal from  $\text{CH}_3$  could, nevertheless, be detected together with that from  $\text{SiF}_2$ . Fig. 2 shows a signal recorded at 200 nm and employing larger reactant concentrations than in Fig. 1. Its magnitude corresponds to the marked decrease of the  $\text{SiF}_2$  absorption cross section with decreasing wavelength as analyzed below and to the absorption cross section of  $\text{CH}_3$  as reported in ref. 18. Fig. 2 indicates that  $[\text{SiF}_2]$  and  $[\text{CH}_3]$  have different time dependences. While  $[\text{CH}_3]$  first increases and then decreases,  $[\text{SiF}_2]$  like in Fig. 1 reaches a stationary final level. The decay of the  $\text{CH}_3$  signal corresponds to the dimerization  $2\text{CH}_3 \rightarrow \text{C}_2\text{H}_6$ , whose rate, under the present conditions, is known.<sup>18</sup> In contrast to  $[\text{CH}_3]$ ,  $[\text{SiF}_2]$  finally remains constant such as shown in Fig. 1. Apparently, the reverse of reactions (1) and (2) do not play a role, such that the signal of Fig. 1 can be attributed to the slower of reactions (1) and (2), in this case, obviously to reaction (1).

### Absorption cross sections of $\text{SiF}_2$

Systematically inspecting final absorption levels of signals like Fig. 1 and 2, high-temperature absorption cross sections of  $\text{SiF}_2$  were derived. Varying the temperature between 1500 and 1900 K (where the reaction was complete within the available observation time of about 1 ms), a major influence of temperature on the final absorption level could not be detected. On the one hand, this proved that the dissociation of  $\text{Si}(\text{CH}_3)_2\text{F}_2$  was complete and no back-reaction took place. The final absorption level was found to be proportional to the reactant concentration which confirmed this conclusion. On the other hand, a temperature dependence of the absorption cross section of  $\text{SiF}_2$  over this temperature range was only small. Slightly varying the wavelength (between 220 and 225 nm) indicated that the room-temperature band structure<sup>12</sup> was absent at the present elevated temperatures and that the  $\text{SiF}_2$  spectrum now indeed was quasi-continuous. Assuming that each decomposing  $\text{Si}(\text{CH}_3)_2\text{F}_2$  produces one  $\text{SiF}_2$ , a maximum absorption cross section  $\sigma(\text{SiF}_2, 222 \text{ nm}) = (2.45 \pm 0.5) \times 10^{-17} \text{ cm}^2$  (base e) was derived for temperatures near 1600 K. Fig. 3



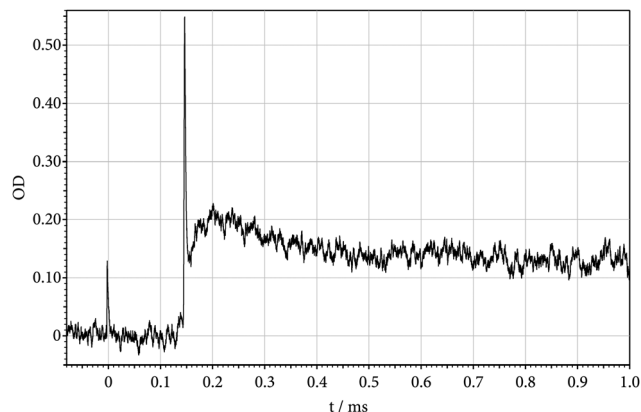


Fig. 2 As Fig. 1, but at 200 nm; superimposed absorptions of  $\text{SiF}_2$  and  $\text{CH}_3$  ( $T = 1720$  K,  $[\text{Ar}] = 8.2 \times 10^{-5} \text{ mol cm}^{-3}$ , 210 ppm of  $\text{Si}(\text{CH}_3)_2\text{F}_2$  in Ar).

shows the results for the wavelength dependence of  $\sigma(\text{SiF}_2, \lambda)$  near 1600 and 3000 K (Table S1 of the ESI† shows experimental values of  $\sigma(\text{SiF}_2, \lambda)$ ). Analogous to the observations for  $\text{CF}_2$  from ref. 9,  $\sigma(\text{SiF}_2, \lambda)$  has a Gaussian shape. The wavelength-integrated absorption cross section  $I(\lambda) = \int \sigma(\text{SiF}_2, \lambda) d\lambda$  (between 195 and 255 nm) is equal to  $4.3 (\pm 1) \times 10^{-23} \text{ cm}^3$ , being close to the value  $5.2 \times 10^{-23} \text{ cm}^3$  derived in ref. 12 from the experimental radiative lifetimes of  $\text{SiF}_2$  from ref. 19.

A representation of the complete wavelength and temperature dependence of  $\sigma$  in Sulzer–Wieland form<sup>20</sup>

$$\sigma(\nu, T) \approx \sigma_{\max} [\tanh(\theta_0/2T)]^{1/2} \exp\{-\tanh(\theta_0/2T) [(\nu - \nu_0)/\Delta\nu_0]^2\} \quad (3)$$

(with  $\nu = 1/\lambda$ ) requires information on the four parameters  $\sigma_{\max}$ ,  $\theta_0$ ,  $\nu_0$ , and  $\Delta\nu_0$ . Fitting the data of Fig. 3 to eqn (3) leads to the parameters  $\sigma_{\max} \approx 2.87 \times 10^{-17} \text{ cm}^2$ ,  $\nu_0 \approx 45045 \text{ cm}^{-1}$ , and  $\Delta\nu_0 \approx 1785 \text{ cm}^{-1}$ . The determination of the parameter  $\theta_0$  requires experiments over larger temperature ranges. In the present case, experiments were extended up to temperatures of 3200 K where  $\text{Si}(\text{CH}_3)_2\text{F}_2$  decomposes in less than a  $\mu\text{s}$ . Fig. 4 shows an example for 3060 K. Instead of staying constant as in

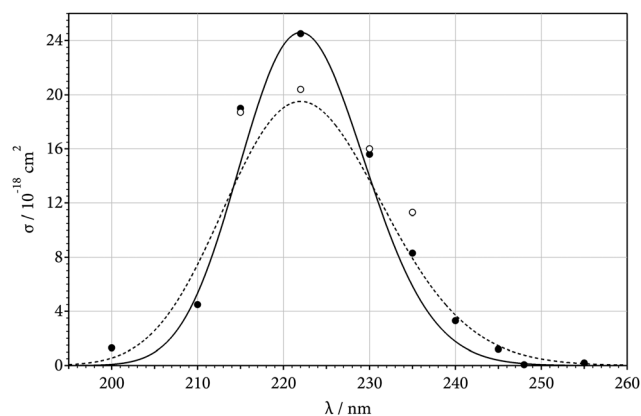


Fig. 3 Absorption cross sections  $\sigma$  of  $\text{SiF}_2$  (experimental points from the present work,  $T$  near 1600 K,  $\bullet$ , and 3000 K,  $\circ$ ; representation of  $\sigma(T)$  by eqn (3) for  $T = 1600$  K, solid line, and 3000 K, dashed line).

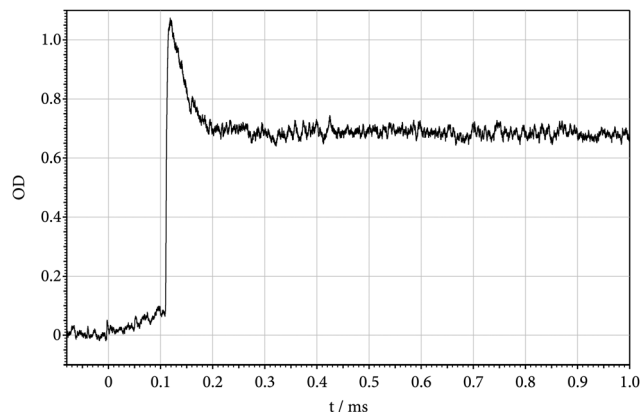


Fig. 4 As Fig. 1, but at higher temperatures (210 ppm of  $\text{Si}(\text{CH}_3)_2\text{F}_2$  in Ar;  $T = 1470$  K and  $[\text{Ar}] = 1.6 \times 10^{-5} \text{ mol cm}^{-3}$  behind incident shock wave;  $T = 3060$  K and  $[\text{Ar}] = 8.1 \times 10^{-5} \text{ mol cm}^{-3}$  behind reflected shock wave; time scale behind incident shock wave compressed by a factor of 3.3).

Fig. 1, the signal here decreases by secondary reactions which will be analyzed later. Nevertheless, the absorption cross section of  $\text{SiF}_2$  can be determined before this decay becomes a problem (e.g., after 10  $\mu\text{s}$  in Fig. 4). Selected results are included in Fig. 3 and compared with a Sulzer–Wieland plot using  $\theta_0 \approx 3000$  K. This value of  $\theta_0$  is relatively uncertain. It is mainly based on measurements at 222 nm and it is definitely larger than the corresponding value<sup>9</sup> for the spectrum of  $\text{CF}_2$  (it should be mentioned that the present results are consistent with values derived from the thermal dissociation of  $\text{SiF}_4$  which will be reported separately, thus supporting the described analysis). It should also be mentioned that absorption-time signals at wavelengths larger than 240 nm increasingly deviate from Fig. 1. Apparently, absorptions from other species here are superimposed on the absorptions from  $\text{SiF}_2$ , such as analyzed below.

### Unimolecular dissociation of $\text{Si}(\text{CH}_3)_2\text{F}_2$

In the second part of our experiments, the kinetics of  $\text{Si}(\text{CH}_3)_2\text{F}_2$  dissociation was explored. The time dependence of the absorption-time profile of Fig. 1 corresponds to a first-order process, i.e.  $[\text{SiF}_2](t) = [\text{Si}(\text{CH}_3)_2\text{F}_2](t = 0) \{1 - \exp(-kt)\}$  with  $k = 8.3 \times 10^3 \text{ s}^{-1}$ . In cases where  $[\text{SiF}_2](t)$  did not approach the final level  $[\text{SiF}_2](t = \infty)$  sufficiently well within the available observation time, i.e. at temperatures below about 1500 K, the initial rate of absorption increase could also be evaluated to derive  $k$ . This required the use of absorption cross sections  $\sigma$  from eqn (3). Then,  $\text{dOD}(t)/\text{d}t = \sigma l [\text{SiF}_2](t = \infty)k$  (with the optical density  $\text{OD} = \sigma l [\text{SiF}_2]$  and the optical path length  $l = 9.4 \text{ cm}$  of our arrangement) also led to rate constants  $k$ . This evaluation was necessary in particular for measurements behind incident shock waves. Fig. 4 shows an example. As our modelling (see the ESI†) predicted an only weak dependence of  $k$  on  $[\text{Ar}]$ , only the comparison of measurements behind incident and reflected shock waves provided a sufficiently large variation of bath gas concentrations to draw meaningful conclusions on the shape of falloff curves  $k([\text{Ar}])$  (the accessible



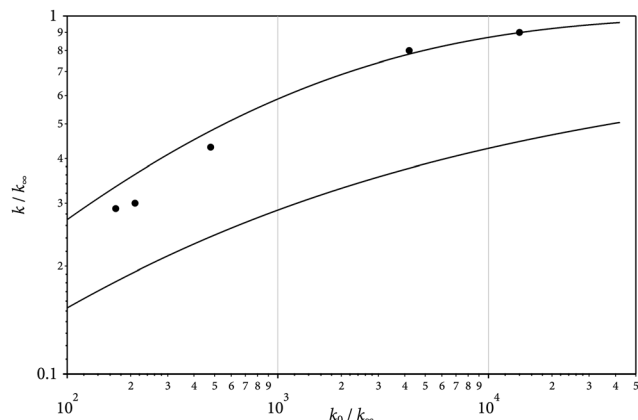


Fig. 5 Doubly-reduced representation of falloff curves  $k([Ar])$  for the unimolecular dissociation of  $Si(CH_3)_2F_2$  (representation of  $k([Ar])/k_\infty$  as a function of  $k_0/k_\infty$  with  $k_0$  from eqn (5) and  $k_\infty$  from eqn (4); upper solid line: modelling with eqn (8), lower solid line: modelling with eqn (7); experimental points from left to right:  $T/K = 1400, 1500, 1600, 1700, 1800$ , respectively).

range was from  $[Ar] \approx 10^{-5} \text{ mol cm}^{-3}$  in incident waves to  $10^{-4} \text{ mol cm}^{-3}$  in reflected waves). Fig. 5 compares two alternative representations of  $k([Ar])$  with experimental results from incident and reflected shock waves (a doubly-reduced representation of  $k/k_\infty$  vs.  $k_0/k_\infty$  was chosen in order to include results from different temperatures; the used  $k_0$  and  $k_\infty$  are from the modelled expressions given below). A more complete representation of experimental data is provided by the Arrhenius plots of Fig. 6 (for constant  $[Ar]$ ; small mismatches of the experimental  $[Ar]$  from the given values were accounted for by the  $[Ar]$ -dependences of Fig. 5; the scatter of about  $\pm 20\%$  of the points in Fig. 5 and 6 is larger than the systematic uncertainty of the measurements). Within the scatter, measured and modelled rate constants agree. As the reaction was studied not far from the high-pressure limit, the agreement mostly confirms the quality of the quantum-chemistry based

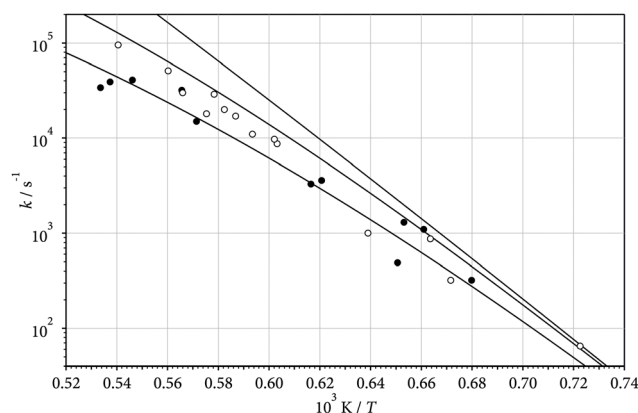


Fig. 6 Arrhenius plots of rate constants  $k(T)$  for the unimolecular dissociation of  $Si(CH_3)_2F_2$  at  $[Ar] \approx 10^{-5}$  ( $\circ$ ) and  $10^{-4}$  ( $\bullet$ )  $\text{mol cm}^{-3}$ , between  $T = 1370$  and  $1890 \text{ K}$  (modelled lines: representation of falloff curves by eqn (8), from bottom to top for  $[Ar] = 10^{-5} \text{ mol cm}^{-3}$ ,  $[Ar] = 10^{-4} \text{ mol cm}^{-3}$ , and  $k_\infty$ , see the ESI†).

calculation of  $k_\infty$  (see the ESI†). Because of the uncertainty of the used collisional energy transfer parameters (see the ESI†), the modelling of the low-pressure rate constants  $k_0$  is less certain. Its influence on the derived high-pressure constants  $k_\infty$ , however, is only weak. In conclusion, the experimental data are remarkably consistent with the high-pressure rate constants such as modelled in the ESI†. These can be expressed by

$$k_\infty = 1.24 \times 10^{19} (T/2000 \text{ K})^{-6.63} \exp(-58400 \text{ K}/T) \text{ s}^{-1} \quad (4)$$

Low-pressure rate constants were modelled as

$$k_0 \approx [Ar] 2.94 \times 10^{25} (T/2000 \text{ K})^{-25.04} \exp(-61980 \text{ K}/T) \text{ cm}^3 \text{ mol}^{-1} \text{ s}^{-1} \quad (5)$$

The representation of the falloff curves of Fig. 5 has employed expressions of the form

$$k([Ar])/k_\infty = [x/(1+x)]F(x) \quad (6)$$

with  $x = k_0/k_\infty$  and “broadening factors”  $F(x)$ . Either “symmetric broadening factors”  $F(x)$  (i.e.,  $F(x) = F(1/x)$ ) of the form proposed in ref. 21,

$$\log F(x) \approx \log F_{\text{cent}}/[1 + (\log x/N)^2] \quad (7)$$

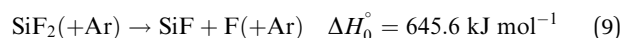
(with  $N \approx 0.75\text{--}1.27 \log F_{\text{cent}}$  and system-specific “center broadening factors”  $F_{\text{cent}}^{22}$ ), or “asymmetric broadening factors”  $F(x)$  (i.e.  $F(x) \neq F(1/x)$ ) were used, the latter being of the form proposed in ref. 14 and 15

$$F(x) \approx (1 + x/x_0)/[1 + (x/x_0)^n]^{1/n} \quad (8)$$

(with  $n = [\ln 2/\ln(2/F_{\text{cent}})] [1 - b + b(x/x_0)^q]$ ,  $q = (F_{\text{cent}} - 1)/\ln(F_{\text{cent}}/10)$ , and the parameters  $x_0$  and  $b$  close to  $x_0 = 1(\pm 0.1)$  and  $b = 0.2(\pm 0.05)$ ). The comparison of the two alternative expressions for falloff curves with the experimental data in Fig. 5 suggests that the asymmetric form of  $F(x)$ , i.e. Eqn (8), near to the high-pressure limit performs much better than the symmetric form of  $F(x)$ , i.e. Eqn (7).

### Kinetics of $SiF_2$ reactions

The experiments described so far, which characterize the formation of  $SiF_2$  (and  $CH_3$ ) in the unimolecular dissociation of  $Si(CH_3)_2F_2$ , finally were extended to higher temperatures where the primary dissociation is so rapidly complete that it cannot be resolved any longer. Fig. 4 gives an example for the reflected shock wave. If only reactions (1) and (2) would take place, the absorption signal behind the reflected shock wave then would remain constant. Instead, one observes a decrease to a new steady level. The decrease of the signal is much faster than expected for the thermal dissociation of  $SiF_2$ , i.e.



(for this reaction, a rate constant of  $k_{9,0} = [Ar] 2 \times 10^{16} (T/1000 \text{ K})^{-1.34} \exp(-72910 \text{ K}/T) \text{ cm}^3 \text{ mol}^{-1} \text{ s}^{-1}$  has been modelled analogous to the calculations described in the present ESI† such that  $SiF_2$  would have a half-life of about 7 s; likewise, the final absorption level of Fig. 4 cannot correspond to a dissociation equilibrium  $SiF_2 \leftrightarrow SiF + F$ ). An unambiguous interpretation of





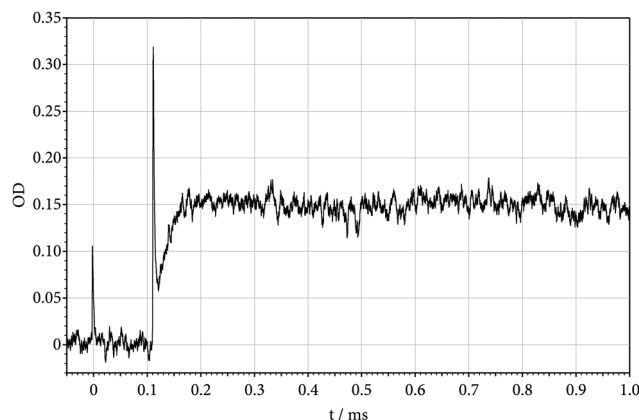
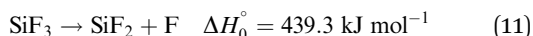


Fig. 7 As Fig. 1, but at 265 nm, showing the formation of SiF in the consumption of SiF<sub>2</sub> by reaction (12) (reflected shock wave with  $T = 3080$  K,  $[\text{Ar}] = 3.8 \times 10^{-5} \text{ mol cm}^{-3}$ , 210 ppm of Si(CH<sub>3</sub>)<sub>2</sub>F<sub>2</sub> in Ar).

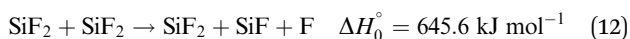
the signal, instead, is provided by measurements at wavelengths where an absorption from SiF<sub>2</sub> can be neglected. Fig. 3 indicates that, even at the temperature of Fig. 4, an absorption signal from SiF<sub>2</sub> should be negligible at wavelengths larger than about 250 nm. Fig. 7 gives an example for a wavelength of 265 nm and nearly the same temperature as in Fig. 4. The initial decay of the SiF<sub>2</sub> signal from Fig. 4 now is mirrored by an absorption increase in Fig. 7. The rate of the initial decay of SiF<sub>2</sub> in Fig. 4 and the formation of a reaction product in Fig. 7 both were found to increase proportional to  $[\text{SiF}_2](t = 0)$ , *i.e.* the observation corresponds to a bimolecular process. In addition, the rate constant for this process was found to have an only small positive temperature coefficient. These observations suggest that SiF<sub>2</sub> is consumed by a reaction



A modelling of the rate constant for unimolecular dissociation of SiF<sub>3</sub> analogous to that described in the present ESI<sup>†</sup> on the other hand, indicates that SiF<sub>3</sub> under the conditions of Fig. 4 and 7 should rapidly dissociate by



The sequence of reactions (10) and (11), *i.e.*



then corresponds to a process which is catalyzed by the reactant SiF<sub>2</sub> and which is much faster than the slow thermal dissociation of SiF<sub>2</sub> by reaction (9). We found no evidence against the assumption that reaction (12) proceeds until SiF<sub>2</sub> is completely consumed and converted to SiF + F. In this case, the final absorption levels of Fig. 4 and 7 can be attributed exclusively to SiF and high-temperature absorption cross sections of SiF can also be derived. Values of  $\sigma/10^{-17} \text{ cm}^2 = 1.0, 2.2, 1.3, 0.9, 0.5, 0.3, 0.4, 0.5, 0.8, 0.6$ , and 0.2 were determined near 3000 K for wavelengths of 200, 210, 220, 230, 240, 250, 260, 270, 280, 290, and 300 nm, respectively. It is known that SiF has numerous band systems from the vacuum-UV to the red (see a summary in ref. 23). At high temperatures, hot bands from these systems overlap into a broad quasi-continuum,

extending beyond that from SiF<sub>2</sub>, but intense enough to be observed. The oscillator strengths of the band systems of SiF and SiF<sub>2</sub> in the ESI<sup>†</sup> were modelled to be of similar magnitude, which appears consistent with the present observations.

Evaluating SiF<sub>2</sub> consumption and SiF formation from experiments like Fig. 7, led to rate constants  $k_{10}$  in the range  $10^{11}$ – $10^{12} \text{ cm}^3 \text{ mol}^{-1} \text{ s}^{-1}$  between  $T = 1900$  and 3500 K, respectively. Experiments with varying reactant concentrations led to similar values which supported the proposed interpretation. One may finally ask for the fate of the F atoms from the net reaction (12). This question could not be answered here. It may be that leftover C<sub>2</sub>H<sub>6</sub> and CH<sub>3</sub> from the precursor act as a sink for these atoms. Evidence for an interference with the described mechanism of reactions (10) and (11) was not found. It should finally be mentioned that absorption signals like Fig. 7 at higher temperatures and higher reactant concentration show a decrease with time, before another increase sets in. These observations are similar as those found in the fluorocarbon system.<sup>11</sup> An analogous interpretation by secondary reactions like  $\text{SiF} + \text{SiF} \rightarrow \text{Si}_2\text{F} + \text{F}$ , followed by  $\text{Si}_2\text{F} \rightarrow \text{Si}_2 + \text{F}$ , would appear possible, but cannot be confirmed at this stage. More details of the suggested autocatalytic reaction sequence of reactions (10) and (11) clearly have to be explored.

## Conclusions

The present work illustrated that the thermal dissociation of Si(CH<sub>3</sub>)<sub>2</sub>F<sub>2</sub> is a suitable source for generating SiF<sub>2</sub> under high-temperature conditions such as studied in shock waves. On the one hand, this allowed to record and calibrate the temperature- and wavelength-dependence of UV absorption cross sections of SiF<sub>2</sub>. The wavelength-integrated absorption cross section here was found to be consistent with the value derived from the radiative lifetime of the species at room temperature.<sup>12</sup> In future work on high-temperature reactions of SiF<sub>2</sub>, the absorption cross sections from eqn (3) will serve for quantitative determinations of SiF<sub>2</sub> concentrations.

In addition to the study of the UV spectrum of SiF<sub>2</sub>, the thermal dissociation of Si(CH<sub>3</sub>)<sub>2</sub>F<sub>2</sub> could be studied under conditions where the reaction is unimolecular. The reaction was found to be not far from its high-pressure limit. A quantum-chemistry based modelling of the rate constant gave results in close agreement with the experiments, which confirmed the reliability of the modelling approach. The falloff curves of the unimolecular reaction could best be represented with asymmetric broadening factors in the form suggested in ref. 14 and 15.

It was finally suggested that the consumption of SiF<sub>2</sub> under the applied conditions did not proceed by thermal unimolecular dissociation, but by an autocatalytic process, *i.e.* via a sequence of the steps  $\text{SiF}_2 + \text{SiF}_2 \rightarrow \text{SiF} + \text{SiF}_3$ , followed by  $\text{SiF}_3 \rightarrow \text{SiF}_2 + \text{F}$ . An analogy to the reaction sequence  $\text{CF}_2 + \text{CF}_2 \rightarrow \text{CF} + \text{CF}_3$ , followed by  $\text{CF}_3 \rightarrow \text{CF} + \text{F}$ , as observed in high-temperature fluorocarbon chemistry appears obvious.



## Conflicts of interest

There are no conflicts of interest to report.

## Acknowledgements

Discussions of this work with Klaus Hintzer and Arne Thaler as well as financial support by the Deutsche Forschungsgemeinschaft (Project TR69/20-1) are gratefully acknowledged. Open Access funding provided by the Max Planck Society.

## References

- 1 V. M. Donnelly, Review article: Reactions of fluorine atoms with silicon, revisited, again, *J. Vac. Sci. Technol., A*, 2017, **35**, 05C202.
- 2 A. C. Stanton, A. Freedman, J. Worthoudt and P. P. Gaspar, Gas phase reactions of SiF<sub>2</sub> with F<sub>2</sub> and Cl<sub>2</sub>, *Chem. Phys. Lett.*, 1985, **122**, 190–195.
- 3 D. R. Harding and D. Husain, Kinetics of SiF(X<sup>2</sup>Π<sub>r</sub>) by time-resolved molecular resonance absorption spectroscopy following the reaction of Si(3<sup>3</sup>P<sub>j</sub>, 3<sup>1</sup>D<sub>2</sub>, 3<sup>1</sup>S<sub>0</sub>), generated by pulse irradiation, with fluorinated compounds, *J. Chem. Soc., Faraday Trans. 2*, 1986, 937–952.
- 4 H. F. Winters and I. C. Plumb, Etching reactions for silicon with F atoms: Product distributions and ion enhancement mechanisms, *J. Vac. Sci. Technol., B*, 1991, **9**, 197–207.
- 5 S. Vanhaelemeersch, J. Van Hoeymissen, D. Vermeylen and J. Peeters, SiF<sub>2</sub> as a primary desorption product of Si etching by F atoms: Interpretation of laser-induced fluorescence spectra; rate constant of the gas phase SiF<sub>2</sub> + F reaction, *J. Appl. Phys.*, 1991, **70**, 3892–3898.
- 6 N. S. J. Braithwaite, J. P. Booth and G. Cunge, A novel electrostatic probe method for ion flux measurements, *Plasma Sources Sci. Technol.*, 1996, **5**, 677–684.
- 7 S. Konieczny, P. P. Gaspar and J. Wormhoudt, Flow pyrolysis of hexafluorodisilane as a source of highly reactive difluoro-silylene, *J. Organomet. Chem.*, 1986, **307**, 151–155.
- 8 S. C. Bains, P. N. Noble and R. Walsh, Kinetics and mechanism of the gas-phase pyrolysis of hexafluorodisilane in the presence of iodine and some reactions of silicon difluoride, *J. Chem. Soc., Faraday Trans. 2*, 1986, 837–847.
- 9 C. J. Cobos, A. E. Croce, K. Luther, L. Sölter, E. Tellbach and J. Troe, Experimental and modeling study of the reaction C<sub>2</sub>F<sub>4</sub> (+M) → CF<sub>2</sub> + CF<sub>2</sub> (+M), *J. Phys. Chem. A*, 2013, **117**, 11420–11429.
- 10 C. J. Cobos, G. Knight, L. Sölter, E. Tellbach and J. Troe, Kinetic and spectroscopic studies of the reaction of CF<sub>2</sub> with H<sub>2</sub> in shock waves, *J. Phys. Chem. A*, 2017, **121**, 7827–7834.
- 11 C. J. Cobos, K. Hintzer, L. Sölter, E. Tellbach, A. Thaler and J. Troe, High-temperature fluorocarbon chemistry revisited, *J. Phys. Chem. A*, 2021, **125**, 5626–5632.
- 12 M. Kogelschatz, G. Cunge and N. Sadeghi, Identification of halogen containing radicals in silicon etching plasmas and density measurement by UV broad band absorption spectroscopy, *J. Phys. D: Appl. Phys.*, 2004, **37**, 1954–1964.
- 13 S. Sharpe, B. Hartnett, H. S. Sethi and D. S. J. Sethi, Absorption cross sections of CF<sub>2</sub> in the A<sup>1</sup>B<sub>1</sub> → X<sup>1</sup>A<sub>1</sub> transition at 0.5 nm intervals and absolute rate constant for 2 CF<sub>2</sub> → C<sub>2</sub>F<sub>4</sub> at 298 K ± 3 K, *J. Photochem.*, 1987, **38**, 1–13.
- 14 J. Troe and V. G. Ushakov, Revisiting falloff curves of thermal unimolecular reactions, *J. Chem. Phys.*, 2011, **135**, 054304.
- 15 J. Troe and V. G. Ushakov, Representation of “broad” falloff curves for dissociation and recombination reactions, *Z. Phys. Chem.*, 2014, **228**, 1–10.
- 16 C. J. Cobos, K. Hintzer, L. Sölter, E. Tellbach, A. Thaler and J. Troe, Shock wave and modelling study of the UV spectra of perfluorocarbon iodides and perfluorocarbon radicals, *Combust. Flame*, 2021, **224**, 177–182.
- 17 R. Roberge, C. Sandorfy, J. I. Matthews and O. P. Strausz, The far ultraviolet and HeI photoelectron spectra of alkyl and fluorine substituted silane derivatives, *J. Chem. Phys.*, 1978, **69**, 5105–5112.
- 18 K. Glänzer, M. Quack and J. Troe, High temperature UV absorption and recombination of methyl radicals in shock waves, *Proc. Combust. Inst.*, 1977, **16**, 949–960.
- 19 J. P. Booth, G. Cunge, F. Neuilly and N. Sadeghi, Absolute radical densities in etching plasmas determined by broadband UV absorption spectroscopy, *Plasma Sources Sci. Technol.*, 1998, **7**, 423–430.
- 20 P. Sulzer and K. Wieland, Intensitätsverteilung eines kontinuierlichen Absorptionsspektrums in Abhängigkeit von Temperatur und Wellenzahl, *Helv. Phys. Acta*, 1952, **25**, 653–676.
- 21 J. Troe, Predictive possibilities of unimolecular rate theory, *J. Phys. Chem.*, 1979, **83**, 114–126.
- 22 J. Troe, Theory of thermal unimolecular reactions in the falloff range. I. Strong collision rate constants, *Ber. Bunsenges. Phys. Chem.*, 1983, **87**, 161–169.
- 23 R. W. B. Pearse and A. G. Gaydon, *The Identification of Molecular Spectra*, 3rd edn, Chapman and Hall, London, 1963.

